Rapid, high-frequency, and theta-coupled gamma oscillations in the inferior occipital gyrus during face processing

Wataru Sato[1,2+], Takanori Kochiyama[1+], Shota Uono[3], Kazumi Matsuda[4], Keiko Usui[4], Yushi Inoue[4], and Motomi Toichi[2,3] ([+] equal contributors)

[1] The Hakubi Project, Primate Research Institute, Kyoto University.

[2] The Organization for Promoting Research in Developmental Disorders.

[3] Faculty of Human Health Science, Kyoto University.

[4] National Epilepsy Center, Shizuoka Institute of Epilepsy and Neurological Disorders.

Abstract

Neuroimaging studies have found greater activation in the inferior occipital gyrus (IOG), or occipital face area, in response to faces relative to non-facial stimuli. However, the temporal, frequency, and functional profiles of IOG activity during face processing remain unclear. Here, this issue was investigated by recording intracranial field potentials in the IOG during the presentation of faces, mosaics, and houses in upright and inverted orientations. Time–frequency statistical parametric mapping analyses revealed greater gamma-band activation in the IOG beginning at 110 ms and covering 40–300 Hz in response to upright faces relative to upright houses and mosaics. Phase–amplitude cross-frequency coupling analyses revealed more evident theta–gamma couplings at 115–256 ms during the processing of upright faces as compared with that of upright houses and mosaics. Comparable gamma-band activity was observed during the processing of inverted and upright faces at about 100–200 ms, but weaker activity and different coupling with theta-band activity after 200 ms. These patterns of activity were more evident in the right than in the left IOG. These results, together with other evidence on neural communication, suggest that broadband gamma oscillations in the right IOG conduct rapid and multistage (i.e., both featural and configural) face processing in collaboration with theta oscillations transmitted from other brain regions.

Keywords: Face; Gamma oscillation; Inferior occipital gyrus; Intracranial field potential recording; Phase–amplitude cross-frequency coupling.

1. Introduction

Faces play an important role in human social interactions owing to the rapid and momentary transmission of various communicative signals from their features/parts (e.g., gaze directions; Kingstone et al., 2000) and configurations/wholes (e.g., emotional facial expressions; McKelvie, 1995). Throughout evolution, the efficient detection and recognition of conspecific faces would have helped humans take collective action in response to biologically important events. Consistent with this notion, behavioral studies have shown that the detection of faces is more rapid compared with that of control stimuli such as houses (e.g., Purcell and Stewart, 1986; Tottenham et al., 2006).

Lesion, stimulation, and neuroimaging studies have found that, in collaboration with other brain regions such as the fusiform gyrus and the superior temporal sulcus, the inferior occipital gyrus (IOG), also known as the occipital face area, plays a crucial role as the neural substrate underlying face processing. Several lesion studies have demonstrated that damage to the IOG induced impaired identity recognition of faces (e.g., Rossion et al., 2003; for a review see Bouvier and Engel, 2006). Likewise, stimulation studies have revealed that electrical activation of the IOG led to various types of impaired face processing including impairments in facial feature perception (e.g., Pitcher et al., 2007), facial configuration perception (Jonas et al., 2012), and the identity recognition of faces (e.g., Allison et al., 1994). Moreover, several neuroimaging studies have reported that the IOG was more active when participants observed faces compared with observing control stimuli such as mosaics and houses (e.g., Liu et al., 2010; Sergent et al., 1992; Strother et al., 2011; for a review, see Pitcher et al., 2011). Because some of these data implicate the IOG in the computationally early stages of face processing, such as the visual analysis of facial features, and because the IOG is the most posterior of the face-related brain regions, some researchers have speculated that the IOG represents the initial stages of a computational hierarchical brain network specific to face processing (e.g., Haxby et al., 2000; Pitcher et al., 2011). However, debate remains regarding this issue because other studies indicate that the IOG is important in the late-stage face processing, such as the visual analysis of facial configuration and facial identity recognition (e.g., Rossion et al., 2011).

Electrophysiological studies can provide valuable information about the neural activity underlying the stages of information processing. Specifically, intracranial electroencephalography

(EEG) can directly record electrical neural activity (field potentials) with high spatial and temporal resolution without the interfering influence of the cranium or scalp in electrical conductance (Mukamel and Fried, 2012). Some previous intracranial EEG studies have recorded the electrical activity of neurons in the IOG or in the adjacent lateral occipital cortex during the processing of faces and other stimuli and have conducted event-related potential (ERP) analyses (Allison et al., 1999; Rosburg et al., 2010; Jonas et al., 2012). These studies have consistently shown that the IOG exhibited stronger activity in response to faces than to other stimuli during the 150–200-ms ERP component, which typically peaked at about 170 ms. Several scalp-recorded EEG studies have shown that this component was the first robust face-specific ERP component identified (e.g., Bentin et al., 1996; for a review, see Rossion and Jacques, 2008). Taken together, these data suggest that the IOG manages initial face-specific neural processing at this stage.

However, an analysis of temporal information in the IOG across broad frequency ranges during face processing is lacking. A previous methodological study showed that the ERP analysis of intracranial EEG recordings detects primarily low-frequency components of the electrical neuronal activity (Edwards et al., 2009). To fully elucidate the high- and low-frequency neuronal activity at high temporal resolution, researchers need to conduct time–frequency analyses (Makeig et al., 2004). A previous intracranial EEG study conducting time–frequency analyses for such activity in the occipital cortex in response to non-facial stimuli identified high-frequency activity related to visual processing at 100–150 ms (Tallon-Baudry et al., 2005). These data suggest that analogous high-frequency activity might be rapidly elicited in the IOG in response to faces.

Among high-frequency neuronal activity, activation in the gamma-band (higher than 30 Hz; e.g., Adrian, 1942) would be of particular interest to the investigation of face-related processing in the IOG. Previous scalp-recorded EEG and magnetoencephalography (MEG) studies have shown that gamma-band neural activity was related to several types of information processing (e.g., Tallon-Baudry et al., 1996; for a review, see Herrmann et al., 2010), including face processing (e.g., Gao et al., 2013). Previous intracranial EEG studies have also identified gamma-band activity during face processing in brain regions other than the IOG (e.g., Engell and McCarthy, 2010; Klopp et al., 1999; Lachaux et al., 2005). Furthermore, because several studies have reported that hemodynamic

responses reflected electrical activity in the gamma band (e.g., Foucher et al., 2003), the face-related activity in the IOG that has been reported in previous neuroimaging studies (e.g., Liu et al., 2010) would be evident in this frequency range. Based on these data, we hypothesized that the IOG would show rapid gamma-band activity during face processing.

Regarding gamma-band neuronal activity, several previous studies have shown that different gamma subbands reflected different functional correlates and microscopic mechanisms (e.g., Edwards et al., 2005; Scheffer-Teixeira et al., 2012; for a review, see Tort et al., 2013). It has been proposed that gamma-band components within the traditionally defined frequency range of 30–100 Hz (Herrmann et al., 2010), as well as a higher range (up to 250 Hz; Edwards et al., 2005), reflect different neural computations (Crone et al., 2006). These data suggest that the IOG might exhibit different patterns of activity across the gamma subbands during face processing.

When considering gamma-band activity in the IOG, its coupling patterns with activity at lower frequency ranges could also be of interest. Several previous studies in humans and animals have shown that gamma-band activity in which the amplitudes were associated with phases of theta-band activity were critically involved in several information processes such as learning and decision making (e.g., Canolty et al., 2006; for a review, see Lisman and Jensen, 2013). Ample evidence suggests that such phase–amplitude cross-frequency coupling between theta and gamma oscillations reflects neural network interactions between long-range inter-regional communications (reflected in theta oscillations) and local intra-regional computations (reflected in gamma oscillations; e.g., Liebe et al., 2012; for reviews, see von Stein and Sarnthein, 2000; Canolty and Knight, 2010). Because several neuroimaging studies have shown that the IOG was functionally coupled with other brain regions during face processing (e.g., Davies-Thompson and Andrews, 2012), we hypothesized that such large-scale functional network patterns would be reflected in theta–gamma cross-frequency coupling in response to faces.

The specific details of face processing by the IOG require further investigation. As mentioned above, debate remains regarding whether the IOG is involved in the early stages of face processing, which includes feature detection, or in the late stages of processing, which includes configuration analysis and identity recognition. Behavioral studies have found that a useful strategy for investigating

face processing involves presenting inverted stimuli (e.g., Yin, 1969; for a review, see Bartlett et al. 2003). A number of studies have shown that the inverted presentation of faces impaired processing due to the difficulty associated with configural/holistic effects (Farah et al., 1995; Mondloch et al., 2002). A previous intracranial EEG study found that, compared with upright presentation, the inverted presentation of faces elicited ERP activity with larger amplitudes and longer peak latencies during the 150–200 ms period in the occipital cortex (Rosburg et al., 2010). These data suggest that low-frequency fluctuations in this time period reflect differences in featural versus configural face processing. However, information processing related to high-frequency activity in the IOG remains untested. Because several lines of evidence implicate the IOG in configural face processing (e.g., Rossion et al., 2011), we hypothesized that IOG gamma-band activity and its association with theta-band activity would be modulated by the inverted presentation of faces.

To identify the time–frequency profile of IOG activity during face processing, an intracranial EEG was recorded from six participants undergoing pre-neurosurgical assessment during the presentation of faces, mosaics, and houses in upright and inverted orientations. In addition to traditional ERP analyses, time–frequency statistical parametric mapping (SPM) was conducted (Kilner et al., 2005). To fully investigate gamma subbands, high-frequency activity up to 300 Hz was analyzed. Furthermore, phase–amplitude cross-frequency coupling analyses were conducted (Voytek et al., 2013). Because several lines of evidence have shown functional hemispheric differences during face processing (e.g., De Renzi al., 1994), the IOG was analyzed in each hemisphere. Based on previous findings, we predicted that the IOG would show stronger broadband gamma-band activity in response to faces than to non-facial stimuli as early as 100 ms, which could be associated with theta-band activity. We also predicted that the presentation of inverted faces would modulate IOG activity.

2. Materials and methods

2.1. Participants

This study included six patients (five females, one male; mean ± *SD* age: 34.5 ± 7.9 years) suffering from pharmacologically intractable focal epilepsy. Intracranial electrodes were implanted in the

patients during the course of pre-surgical evaluation, and electrophysiological and surgical examination revealed that the main epileptic foci were in the hippocampus for five participants and the anterior lateral temporal cortex for one participant. The experiment was conducted 2.0–2.8 weeks after electrode implantation while the participants were receiving a series of neuropsychological and electrophysiological assessments. Neuropsychological assessment confirmed that language abilities and episodic memory functions remained intact in all participants. The intelligence quotient (IQ), measured by the Wechsler Adult Intelligence Scale-Revised, was in the normal range for five participants, and the sixth participant was in the mildly retarded range (mean ± *SD* full-scale IQ: 91.8 ± 19.2; mean ± *SD* verbal IQ: 86.7 ± 12.0; mean ± *SD* performance IQ: 100.7 ± 27.3). During the experiment, no seizure activity was observed, and all participants were mentally stable. All participants were right-handed as assessed using the Edinburgh Handedness Inventory (Oldfield, 1971), possessed normal or corrected-to-normal visual acuity, and provided written informed consent following a full explanation of the procedure. This study was approved by the local institutional ethics committee. The data from different electrodes were reported elsewhere (Sato et al., 2012).

2.2. Anatomical assessment

Pre- and post-implantation anatomical assessments were conducted using structural magnetic resonance imaging (MRI) on a 1.5-T scanning system (Signa TwinSpeed, General Electric Yokokawa) using T-1 weighted images. Three-dimensional fast spoiled gradient-recalled acquisition was utilized with the following parameters: repetition time = 12 ms, echo time = 5 ms, flip angle = 20°, matrix size = 256 x 256, field of view = 22 x 22 cm, and 76 slices resulting in voxel dimensions of 0.8594 x 0.8594 x 2.0 mm thick. Pre-implantation MRI assessments and surgical evaluations did not reveal any structural abnormalities in the bilateral IOG of any participant.

The implantation of intracranial electrodes was performed using the stereotactic method (Mihara and Baba, 2001), and implantation sites were chosen based solely on clinical criteria. Subdural electrodes were implanted in the usual manner in both hemispheres for five participants and in the right hemisphere for one participant.

The electrodes of interest in the IOG region were selected based on anatomical and functional criteria. First, post-implantation anatomical MRI assessments were conducted to confirm the positions

of the electrodes. Individual MRI data were segmented into gray and white matter tissue to create the cortical surface rendering using the unified segmentation and normalization procedure (Ashburner and Friston, 2005) in SPM8 (http://www.fil.ion.ucl.ac.uk/spm/) implemented in MATLAB 7.12 (Mathworks). The susceptibility artifact of each electrode was well visualized in the original MRI and the surface rendering image. One of the authors manually localized the electrodes in the IOG and measured the coordinates by viewing anatomical data using MRIcron software (http://www.mccauslandcenter.sc.edu/mricro/mricron/). This anatomical assessment showed that there were two candidate electrodes in each hemisphere in every patient. Then, we selected a single electrode from each hemisphere of each participant that showed larger amplitude peak negativity during 100–200 ms after stimulus onset in response to faces as compared with mosaics. This functional criterion was adopted because our aim was to investigate the time–frequency profile of IOG activity that showed face-related ERP as reported previously (e.g., Allison et al., 1999). To report the stereotactic coordinates of the electrode positions, the individual MRI was normalized to the standard stereotactic space defined by the Montreal Neurological Institute (MNI) using the unified segmentation and normalization procedure. The spatial transformation parameters from this normalization process were then applied to each of the electrode coordinates. The mean ± *SD* MNI coordinates of the electrode located in the IOG were: Left, x –54.0 ± 3.6, y –71.0 ± 5.2, z 1.3 ± 7.3; Right, x 52.4 ± 6.4, y –73.6 ± 9.1, z –3.0 ± 8.8. Finally, the mean 3D locations of the electrodes were projected on the MNI glass brain (SPM maximum intensity projection format; Fig. 1). The resulting six right and five left IOG electrodes were subjected to the following signal processing and statistical analyses.

2.3. Stimuli

Face stimuli were created using grayscale photographs (Fig. 2) and consisted of images of the full-face neutral expressions of seven female and seven male Japanese models. The stimuli were 200 x 200 pixels in size. The mosaic stimuli were constructed by dividing all face stimuli into 625 squares with 8 x 8 pixels, which were then randomly reordered using a constant algorithm, resulting in stimuli that were unrecognizable as faces. The house stimuli consisted of photographs of 14 houses of the same size as the face stimuli. Under the inverted condition, all of these photographs were used upside down.

The mean luminance for all images was held constant using MATLAB 6.5 (Mathworks).

2.4. Procedure

The presentation of stimuli was controlled by SuperLab Pro 2.0 (Cedrus) and implemented on a Windows computer (FSA600, Teknos). The stimuli were presented on a 19-inch CRT monitor (GDM-F400, Sony) with a refresh rate of 100 Hz and a resolution of 1024 x 768 pixels. The stimuli subtended a visual angle of 7.6°x 7.6°. The responses of participants were recorded using a response box (RB-400, Cedrus).

Experiments were conducted individually in a quiet room. Each participant was seated comfortably 0.57 m from the monitor with her/his head supported by a chin-and-forehead rest.

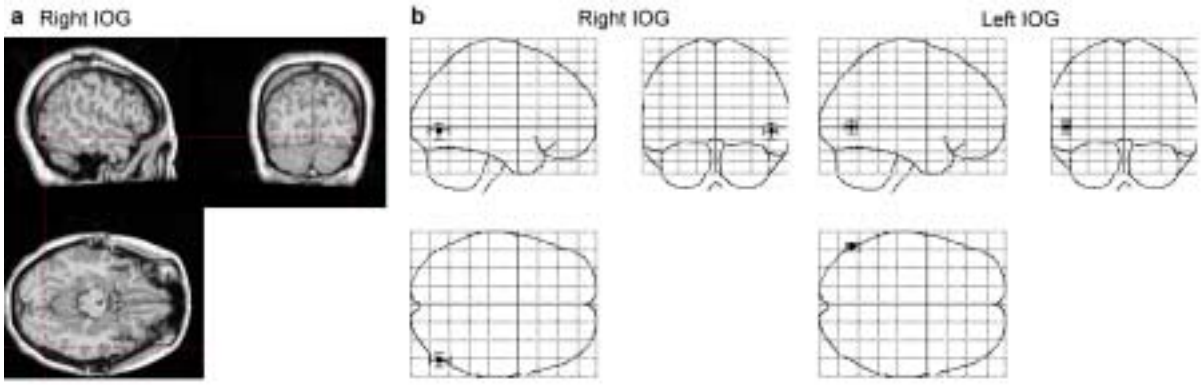

Fig. 1. (a) Representative anatomical MRI. The red cross indicates the location of the IOG electrodes. (b) Mean (± *SD*) coordinates of electrodes in the IOG in the MNI space.

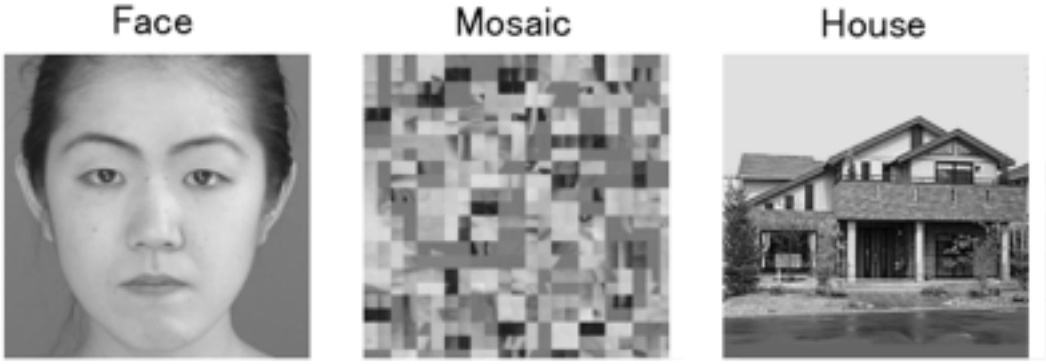

Fig. 2. Examples of stimuli presented to participants.

Each stimulus was presented twice. Additionally, a red cross was presented as the target in 20 trials, yielding a total of 188 trials for each participant (28 trials each for the upright face, upright mosaic, upright house, inverted face, inverted mosaic, and inverted house stimuli as well as 20 target trials). Stimuli were presented in a random order. In each non-target trial, the stimulus was presented centrally for 1,000 ms after a small black cross (0.5°x 0.5°) appeared at a fixation point for 500 ms. In each target trial, the big red cross (1.2°x 1.2°) was presented instead of the photo stimulus until the participants responded. Participants were asked to detect a red cross and then to press a button with the right forefinger as quickly as possible. These dummy tasks confirmed that participants were attending to the stimuli but did not require controlled cognitive, emotional, or behavioral processing of the stimuli. Performance on the dummy target-detection task was perfect (correct identification rate = 100.0%; mean ± *SD* reaction times: 403.1 ± 28.8 ms). Participants were also instructed not to blink while stimuli were being presented. The inter-trial interval varied randomly between 2,000 and 5,000 ms. To avoid habituation and drowsiness, participants were given a short rest upon completion of 25% of the trials. Before data collection, the participants were familiarized with the procedure via training in a block of 10 trials.

2.5. Data recording

Intracranial field potential recording was conducted using subdural platinum electrodes (2.3 mm diameter; Ad-tech) to record cortical activity. Depth platinum electrodes (0.8 mm diameter; Unique Medical) were also inserted to record subcortical activity (data are not shown). Electrodes were referenced to electrodes (2.3 mm diameter; Ad-tech) that were embedded inside the scalp of the midline dorsal frontal region. Impedances were balanced and maintained below 5 kΩ. Data were amplified, filtered online (band pass: 0.5–300 Hz), and sampled at 1,000 Hz onto the hard disk drive of the EEG system (EEG-1100; Nihon Kohden). Online monitoring was conducted with a more restricted bandwidth of 0.5–120 Hz). Vertical and horizontal electrooculograms (EOGs) were simultaneously recorded using Ag/AgCl electrodes (Nihon Kohden). As in previous studies (Lachaux et al., 2003), off-line visual inspection confirmed that no contamination of EOGs by intracranial field potentials had occurred. An unobtrusive video recording of events was made using a built-in video camera of the EEG system, and off-line analysis of the videos confirmed that all participants were fully engaged in

the tasks.

2.6. Data analysis: Preprocessing

Preprocessing, ERP analyses, and time–frequency SPM analyses were performed using SPM8 (http://www.fil.ion.ucl.ac.uk/spm) implemented in MATLAB 7.12 (Mathworks).

Data obtained during 3,000 ms were sampled for each trial; pre-stimulus baseline data were collected for 1,000 ms and experimental data were collected for 2,000 ms after stimulus onset at a sampling rate of 1,000 Hz. Epochs containing signals for which the amplitude was > ± 800 μV were first excluded, and then any epoch with an absolute signal amplitude value >5 *SD* from the mean or median signal amplitude for each electrode for each participant was rejected as an artifact. The frequencies of artifact-contaminated trials did not differ across upright face, upright mosaic, upright house, inverted face, inverted mosaic, or inverted house conditions for either hemisphere (mean ± *SD* = 5.1 ± 1.7% and 5.2 ± 2.1% for the right and left IOG electrodes, respectively; $p > .44$, two-way repeated-measures analysis of variance (ANOVA)).

2.7. Data analysis: ERP

ERP analyses were conducted for IOG activity in each hemisphere. To analyze ERP, 1D SPM analysis (Oswal et al., 2012; Sato et al., 2012), a variant of the 3D sensor-space–time SPM approach (Kilner and Friston, 2010; Litvak et al., 2011), was utilized. Because this study focused on a single electrode, the 3D sensor-space–time SPM was reduced to the single-sensor–time SPM. Single trial responses from all trials for all participants were converted into line images after baseline correction for the -200–0 ms time period. The line images were then entered into the general linear model (GLM) based on a fixed-effects analysis of the pooled error from all trials for all participants. The GLM included stimulus type (face, mosaic, or house), presentation condition (upright or inverted), and laterality (right or left) as factors of interest and participant blocks (six participants) as a factor of no interest. The time window of interest was restricted to 0–500 ms using explicit masking.

To ensure the assumption of an independent and identically distributed error for the GLM, corrections for non-sphericity were applied. The covariance components were modeled to represent dependency and uneven variance between levels. Covariance components were estimated from the pooled whole bins using the restricted maximum likelihood procedure (Friston et al., 2002), and the

inverse of the square root of the estimated covariance matrix was used to pre-whiten the data and design matrix. The least-squares estimation was performed on the whitened data and design matrix, resulting in the maximum likelihood parameter estimates. Finally, 1D SPM{*T*} data were calculated for each contrast.

Planned contrasts were performed to detect significant positive and negative deflections between upright faces and upright mosaics, between upright faces and upright houses, between upright and inverted faces, between inverted faces and inverted mosaics, and between inverted faces and inverted houses for each hemisphere. We further tested the differences across the hemispheres for these contrasts by analyzing interactions between stimulus conditions (e.g., upright faces versus upright mosaics) and laterality (e.g., right versus left); inclusive masks were applied to avoid false deactivations by subtraction. Statistical inferences on 1D SPM{*T*} data were based on random field theory (Kilner and Friston, 2010; Worsley et al., 1996). Significant responses were identified using an extent threshold of $p < .05$, corrected for multiple comparisons over the whole post-stimulus time (0–500 ms), with a height threshold of $p < .001$ (uncorrected).

2.7. Data analysis: Time–frequency SPM analysis

Time–frequency SPM analyses (Kilner et al., 2005) were performed for IOG activity in each hemisphere. The time–frequency (power) maps were first calculated for each trial using continuous wavelet decomposition with seven-cycle Morlet wavelets during the whole epoch (-1000–2000 ms) and from 4 to 300 Hz, which covered theta (4–8 Hz), alpha (8–12 Hz), beta (12–30 Hz), traditional gamma (30–100 Hz), and high gamma (100–300 Hz) activity. The time–frequency maps were then cropped to -200–500 ms within the studied time period to prevent edge effects of the wavelet transformation. Finally, the time–frequency maps were log-transformed and baseline-corrected with respect to mean power over the 200 ms pre-stimulus period separately for each frequency.

The time–frequency maps were converted into 2D images and then entered into the GLM in the same manner as the above 1D SPM analysis. The window of interest was restricted to whole frequency ranges (4–300 Hz) during the post-stimulus period (0–500 ms) using explicit masking.

Statistical inferences performed on the time–frequency SPM{*T*} data were based on random field theory (Worsley et al., 1996; Kilner et al., 2005). Based on our interests, the contrast of upright faces

versus upright mosaics, upright faces versus upright houses, upright faces versus inverted faces, and inverted faces versus upright faces were tested for each hemisphere. Significantly activated time–frequency clusters were identified if they reached the extent threshold of $p < .05$, which was corrected for multiple comparisons over the whole time–frequency space (0–500 ms and 4–300 Hz), with a height threshold of $p < .001$ (uncorrected). The equivalent SPM{Z} value was used to report the inferential results. Because the temporal resolution of low-frequency activity is generally poor in time–frequency analyses, the onset latencies are only discussed for high-frequency activity.

2.8. Data analysis: Cross-frequency coupling

The phase–amplitude cross-frequency coupling between theta- and gamma-band activities was analyzed using an event-related phase–amplitude cross-frequency coupling procedure (Voytek et al., 2013). The attractive feature of this procedure is that it can capture dynamic changes in cross-frequency coupling over both temporal and frequency domains, unlike other existing methods (for a review, see Canolty and Knight, 2010). Hence, it was well-suited to the current study, which examined the temporal profile of event-related theta–gamma coupling and related frequency characteristics in the gamma subbands under different conditions.

All analyses were performed using the ERPAC toolbox (http://darb.ketyov.com/professional/publications/erpac.zip), the EEGLAB toolbox (Delorme and Makeig, 2004), and auxiliary in-house programs implemented in MATLAB 7.12 (Mathworks).

The analyses were conducted in three steps. First, the data for each electrode were narrow band-pass filtered using a two-way least-squares finite impulse response procedure (Delorme and Makeig, 2004). The first pass band was set at the theta band (4–8 Hz), and the second at the gamma band was successively changed from 30 to 300 Hz in steps of 10 Hz. Second, a Hilbert transform was applied to the band-pass filtered data. From the results, the theta phases and gamma analytic amplitudes were computed. Third, the circular-linear correlation (Berens, 2009) between the theta phase and gamma analytic amplitude was assessed across trials for each condition at each time point. This analysis corresponded to a regression analysis at each time point to determine the amount of trial-by-trial variance in the gamma amplitude that could be explained by trial-by-trial variation in the theta phase. This processing returned the coupling value between 0 and 1 for each time point, where

‘0’ or ‘1’ meant that the phase and amplitude values were entirely desynchronized or synchronized, respectively. To create the cross-frequency coupling map, this procedure was repeatedly conducted along with extracting the gamma power time series for given frequency bands in the range 30–300 Hz in 10 Hz steps.

For statistical inferences, the significance of the cross-frequency coupling values for each condition was first evaluated. Then, the differences in the values between conditions were compared. Based on our interests, the comparisons of upright faces versus upright mosaics, upright faces versus upright houses, upright faces versus inverted faces, inverted faces versus upright faces, inverted faces versus inverted mosaics, and inverted faces versus inverted houses were tested for each hemisphere. Interaction analyses were not conducted because such ANOVA-type analyses are not yet supported by the current method (Voytek et al., 2013). Statistical inferences for cross-frequency coupling values were based on a permutation test, where a surrogate data method (Lachaux et al., 1999) was used to derive the *z*-score. One thousand surrogate data were generated by shuffling the trials within the gamma analytic amplitude data set. The cross-frequency coupling value was then computed for all surrogate data, resulting in a distribution of cross-frequency coupling values at each time point. The *z*-score was obtained at each time point by subtracting the mean of the surrogate distribution of cross-frequency coupling values from the real cross-frequency coupling value and then dividing by the *SD* of the surrogate distribution. These procedures were separately applied for each gamma-band frequency (30–300 Hz in steps of 10 Hz) to construct the statistical map of the time–frequency cross-frequency coupling. The resulting statistical map was corrected for multiple comparisons over the whole time–frequency space (0–500 ms and 30–300 Hz) using a false discovery rate method, as in a previous study (Voytek et al., 2013). Significant values were identified with a height threshold of $p < .05$ (corrected) and an extent threshold of 100 time-frequency clusters (voxel size: 1 ms x 10 Hz).

3. Results

3.1. ERP

ERP analyses were conducted on IOG activity to compare the current results with findings from previous studies (e.g., Jonas et al., 2012). A visual inspection of grand-average ERP waveforms (Fig.

3) indicated that upright faces, compared with upright mosaics and upright houses, elicited a clear negative deflection, peaking at about 170 ms in the right IOG. Compared with upright faces, inverted faces resulted in a negative deflection with a higher amplitude and longer peak latency at about 190 ms. The ERPs were analyzed using the GLM, including the effects of stimulus type, presentation condition, and laterality (Table 1).

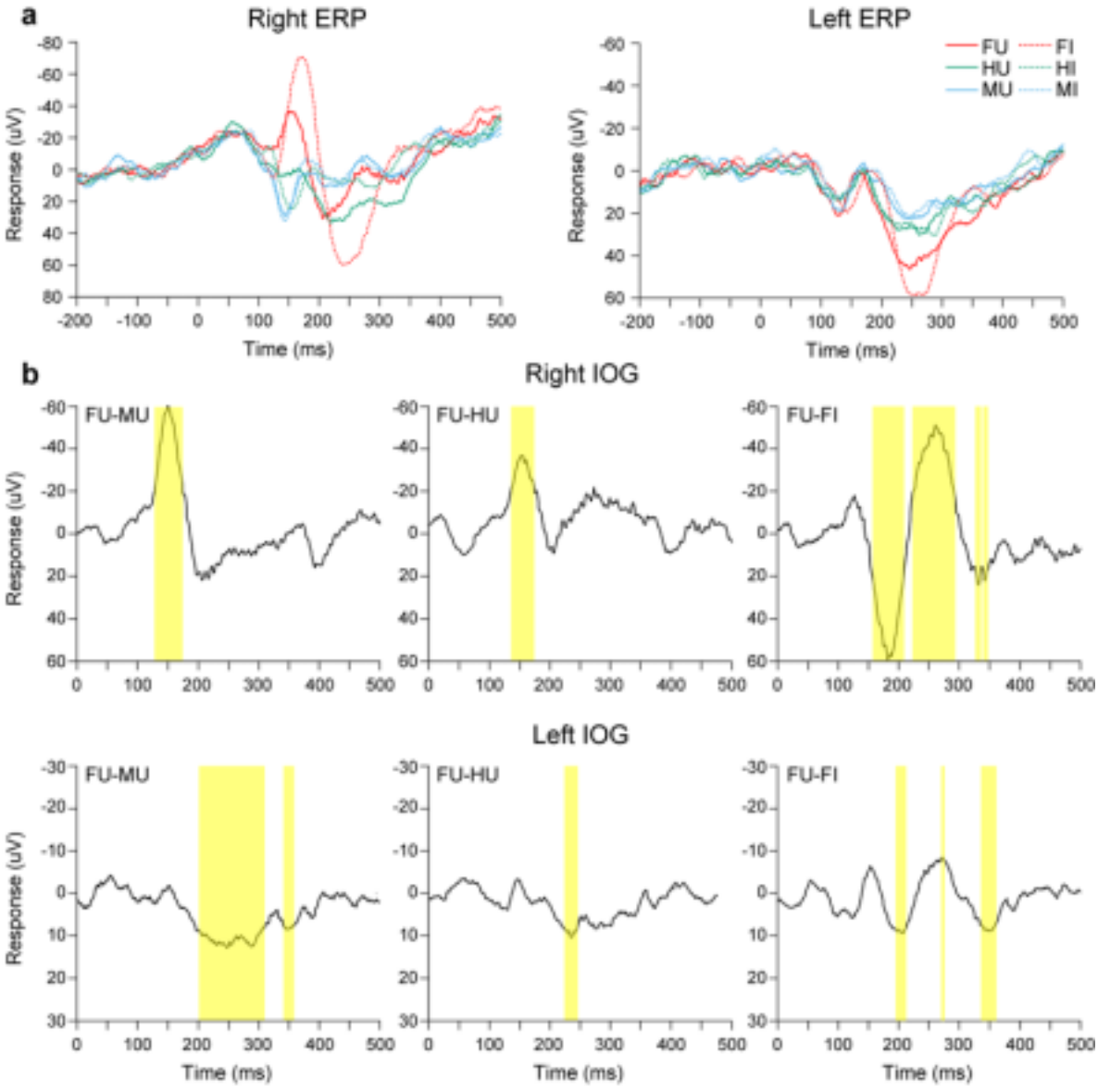

Fig. 3. (a) Grand-average ERP waveforms of IOG activity. FU = upright face; MU = upright mosaic; HU = upright house; FI = inverted face; MI = inverted mosaic; HI = inverted house. (b) Contrasted (differential) ERP waveforms of IOG activity. Colored regions indicate significant difference.

Table 1. ERPs showing significant IOG activity.

		Activation Profile			
		Peak		Extent	
Hemisphere	Contrast	Time (ms)	Z-Value	Time (ms)	Cluster Size (ms)
R	FU - MU	151	8.33	130–175	46
	FU - HU	156	5.30	138–175	38
L	FU - MU	249	4.70	203–311	109
		349	3.55	343–359	17
	FU - HU	249	3.87	237–258	22
R	FU - FI	262	9.22	224–293	70
		183	8.42	158–209	52
		332	4.35	328–336	9
		343	4.08	340–347	8
L	FU - FI	352	3.76	337–361	25
		207	3.48	196–212	17
		273	3.28	271–276	6
R	FI - MI	158	8.01	135–197	63
		265	7.67	216–295	80
	FI - HI	167	8.20	140–198	59
		243	7.39	217–286	70
L	FI - MI	277	7.28	221–301	81
	FI - HI	251	6.35	230–288	59

R = right; L = left.

FU = upright face; MU = upright mosaic; HU = upright house; FI = inverted face; MI = inverted mosaic; HI = inverted house

First, the face-specific activity of the IOG in each hemisphere was investigated using the contrasts of upright faces versus upright mosaics and upright faces versus upright houses. In the right IOG, these contrasts consistently revealed significant negative deflections at 138–175 ms. In the left IOG, both of these contrasts induced significant activation at later positive deflections at 237–258 ms. Second, the effect of the presentations of inverted faces was tested using contrast of upright versus inverted faces and inverted versus upright faces. In the right IOG, the contrast of upright versus inverted faces revealed significant positive deflections at 328–347 ms. The contrast of inverted versus upright faces resulted in significant activation in the right IOG, with a negative deflection at 158–209 ms and a positive deflection at 224–293 ms. Similarly, in the left IOG, the contrast of upright versus inverted faces was associated with a significant positive deflection during the 337–361 ms interval.

The contrast of inverted versus upright faces showed significant activation in the left IOG, with a negative deflection at 196–212 ms and a positive deflection at 271–276 ms.

To test the response to inverted faces, we also contrasted inverted faces versus inverted mosaics and inverted faces versus inverted houses. In the right IOG, these contrasts consistently revealed significant positive deflections at 217–286 ms. Also in the left IOG, these contrasts commonly revealed significant positive deflections during the 230–288 ms interval.

Finally, to explore hemispheric functional asymmetry, the interaction contrasts were tested regarding the above contrasts (Table 2). Significantly higher negative deflections were consistently found in the right than in the left IOG across upright faces versus upright mosaics and houses at 138–158 and 161–165 ms. The contrast of upright versus inverted faces revealed significant activity in negative deflection at 158–198 ms and positive deflection at 224–275 ms in the right versus left IOG. As in the case of upright faces, the contrasts of inverted faces versus inverted mosaics and houses showed a significantly higher negative deflection in the right versus left IOG at 140–193 ms.

Table 2. ERPs showing significant interaction in IOG activity.

	Activation Profile			
	Peak		Extent	
Contrast	Time (ms)	Z-Value	Time (ms)	Cluster Size (ms)
{(R FU - R MU) - (L FU - L MU)}	151	6.26	131–175	45
{(R FU - R HU) - (L FU - L HU)}	148	3.49	138–158	21
	163	3.38	161–165	5
{(L FU - L MU) - (R FU - R MU)}		n.s.		
{(L FU - L HU) - (R FU - R HU)}	252	4.01	239–258	20
{(R FU - R FI) - (L FU - L FI)}		n.s.		
{(R FI - R FU) - (L FI - L FU)}	183	5.81	158–198	41
	262	4.62	224–275	52
{(L FU - L FI) - (R FU - R FI)}		n.s.		
{(L FI - L FU) - (R FI - R FU)}		n.s.		
{(R FI - R MI) - (L FI - L MI)}	159	8.01	136–196	61
{(R FI - R HI) - (L FI - L HI)}	161	7.89	140–193	54
	226	3.72	218–236	19
{(L FI - L MI) - (R FI - R MI)}		n.s.		
{(L FI - L HI) - (R FI - R HI)}		n.s.		

R = right; L = left.

FU = upright face; MU = upright mosaic; HU = upright house; FI = inverted face; MI = inverted mosaic; HI = inverted house

3.2. Time–frequency SPM

To reveal the temporal and frequency profile of IOG activity during face processing, time–frequency SPM analyses were conducted (Fig. 4). The time–frequency maps for IOG activity were analyzed using the GLM using the same factors as the above ERP analyses (Table 3).

First, the face-specific activity of the IOG in each hemisphere was investigated using the contrasts of upright faces versus upright mosaics and upright faces versus upright houses. In the right IOG, these contrasts consistently revealed significant rapid and broadband gamma-band activity spanning 110–500 ms and 40–269 Hz. In the left IOG, these contrasts consistently induced significant gamma-band activity spanning 220–250 ms, 74–93 Hz.

Second, to test the effects of face inversion, contrasts for upright versus inverted faces and inverted versus upright faces were conducted. The contrast of upright versus inverted faces was associated with significant broadband (40–237 Hz) gamma-band activity in the right IOG at 195–500 ms. The contrast of inverted versus upright faces showed two significant clusters of theta/alpha-band activation in the right IOG during 0–406 ms. The contrast of upright versus inverted faces and inverted versus upright faces did not result in any significant activation in the left IOG.

To test the response to inverted faces, we also contrasted inverted faces versus inverted mosaics and inverted faces versus inverted houses. In the right IOG, as in the case of upright faces, these contrasts consistently revealed significant, broadband gamma-band activity spanning 116–409 ms, 47–291 Hz. In the left IOG, there was no significant activation consistently across these two contrasts.

Finally, to test the hemispheric functional asymmetry, the interaction contrasts were tested regarding the above contrasts (Table 4). The results showed that significantly higher activities were found in the right versus left IOG in all of the aforementioned activation clusters in the right IOG, except for the theta/alpha-band activity for inverted versus upright faces. No significant activation was found for the higher activity in the left as compared with the right IOG.

3.3. Cross-frequency coupling

To evaluate the theta–gamma coupling patterns of IOG activity during face processing, event-related phase–amplitude cross-frequency coupling analyses were conducted for the right (Fig. 5) and left (Supplementary Fig. 1) IOG (Table 5).

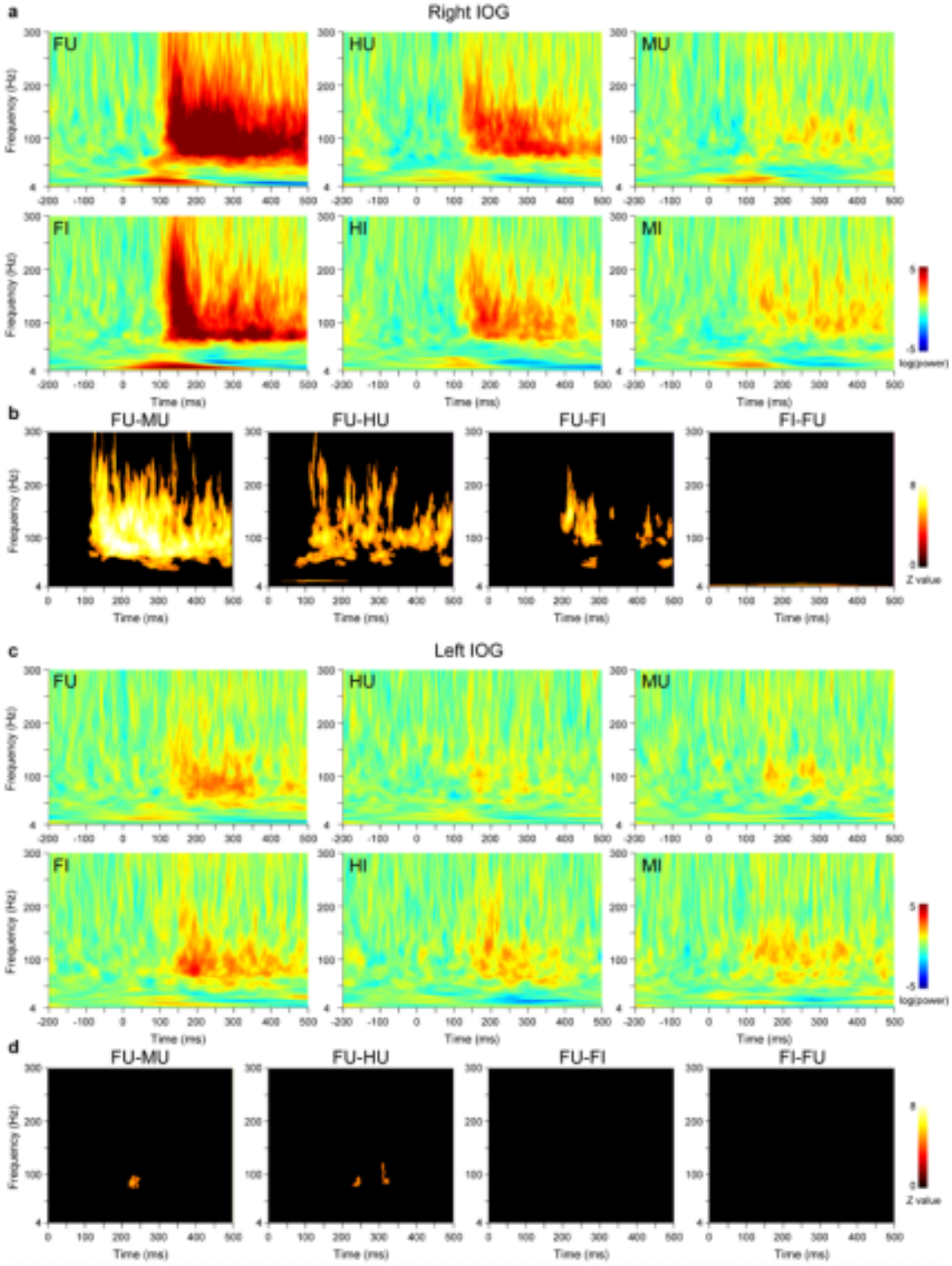

Fig. 4. (a) Time–frequency maps of right IOG activity. FU = upright face; MU = upright mosaic; HU = upright house; FI = inverted face; MI = inverted mosaic; HI = inverted house. (b) Statistical parametric maps for contrasts of right IOG activity. (c) Time–frequency maps of left IOG activity. (d) Statistical parametric maps for contrasts of left IOG activity.

Table 3. Time–frequency regions showing significant IOG activity.

		Activation Profile					
		Peak			Extent		
Hemisphere	Contrast	Time (ms)	Frequency (Hz)	Z-Value	Time (ms)	Frequency (Hz)	Cluster Size (ms x Hz)
R	FU - MU	290	83	8.94	110–500	36–300	58162
		381	300	4.47	380–387	265–300	181
	FU - HU	152	93	6.28	46–500	40–269	34585
		124	260	4.69	110–129	155–300	1214
		481	57	4.43	463–500	43–67	569
		126	14	4.38	13–218	12–16	449
		200	49	3.94	181–211	44–54	233
L	FU - MU	227	82	4.41	220–250	70–95	499
	FU - HU	240	77	4.02	225–250	74–93	237
		320	82	3.96	308–328	78–118	328
R	FU - FI	220	145	7.44	195–307	80–237	7408
		438	110	4.92	402–447	78–167	1344
		279	56	4.49	252–294	40–61	583
		484	49	4.48	459–500	40–57	535
		472	91	4.47	456–485	82–99	314
		336	147	4.33	330–341	133–157	220
		499	117	4.16	483–500	95–137	485
		461	130	3.99	454–471	117–145	229
	FI - FU	281	8	4.82	0–406	5–9	1000
		436	4	3.35	304–486	4	138
L	FU - FI			*n.s.*			
	FI - FU			*n.s.*			
R	FI - MI	205	67	7.34	116–500	47–291	25211
		170	7	7.31	0–360	4–14	2151
		194	257	5.65	190–197	227–300	381
		375	193	4.35	369–377	371–374	211
	FI - HI	148	111	6.94	69–409	46–300	15620
		135	5	6.47	0–420	4–15	
		463	66	6.30	420–500	59–114	
		295	121	3.90	285–301	97–136	265
L	FI - MI	190	78	4.13	163–205	68–86	341
		180	7	3.34	120–293	7	174
	FI - HI			*n.s.*			

R = right, L = left.

FU = upright face, MU = upright mosaic, HU = upright house, FI = inverted face,

MI = inverted mosaic, HI = inverted house

Table 4. Time–frequency regions showing significant interaction in IOG activity.

Contrast	Activation Profile					
	Peak			Extent		
	Time (ms)	Frequency (Hz)	Z-Value	Time (ms)	Frequency (Hz)	Cluster Size (ms x Hz)
{(R FU - R MU) - (L FU - L MU)}	253	120	6.60	133–317	62–252	14401
	374	84	6.23	350–500	55–164	6224
	324	166	5.62	296–342	139–209	1425
	119	121	4.26	117–131	111–143	289
	331	106	4.04	322–337	90–111	206
	343	70	3.99	329–351	65–75	183
	120	250	3.96	118–124	221–274	236
	437	174	3.79	430–442	132–206	361
{(R FU - R HU) - (L FU - L HU)}	150	97	4.59	138–178	85–112	583
	381	93	4.56	352–405	81–114	694
	213	162	4.30	209–219	151–192	243
	271	191	4.20	270–275	159–212	208
	145	243	4.14	138–149	191–261	480
	420	113	4.04	414–431	98–127	312
	237	135	3.88	233–242	111–161	197
{(L FU - L MU) - (R FU - R MU)}			n.s.			
{(L FU - L HU) - (R FU - R HU)}			n.s.			
{(R FU - R FI) - (L FU - L FI)}	220	145	5.19	192–234	109–180	1282
	420	85	4.67	401–431	77–121	381
	241	113	4.44	229–267	96–177	1164
	286	101	4.40	273–299	86–115	474
{(R FI - R FU) - (L FI - L FU)}			n.s.			
{(L FU - L FI) - (R FU - R FI)}			n.s.			
{(L FI - L FU) - (R FI - R FU)}			n.s.			
{(R FI - R MI) - (L FI - L MI)}	143	163	6.40	126–203	83–275	5415
	355	68	5.01	306–371	55–82	893
	469	68	4.77	450–489	61–76	434
	282	66	4.64	186–296	53–79	1175
	361	119	4.19	357–373	105–130	253
	139	67	4.09	122–153	61–76	279
{(R FI - R HI) - (L FI - L HI)}	147	115	5.63	127–167	101–141	2521
	82	5	4.89	0–375	5–6	379
	143	274	4.12	141–146	242–300	228
{(L FI - L MI) - (R FI - R MI)}			n.s.			
{(L FI - L HI) - (R FI - R HI)}			n.s.			

R = right; L = left.

FU = upright face; MU = upright mosaic; HU = upright house; FI = inverted face;

MI = inverted mosaic; HI = inverted house.

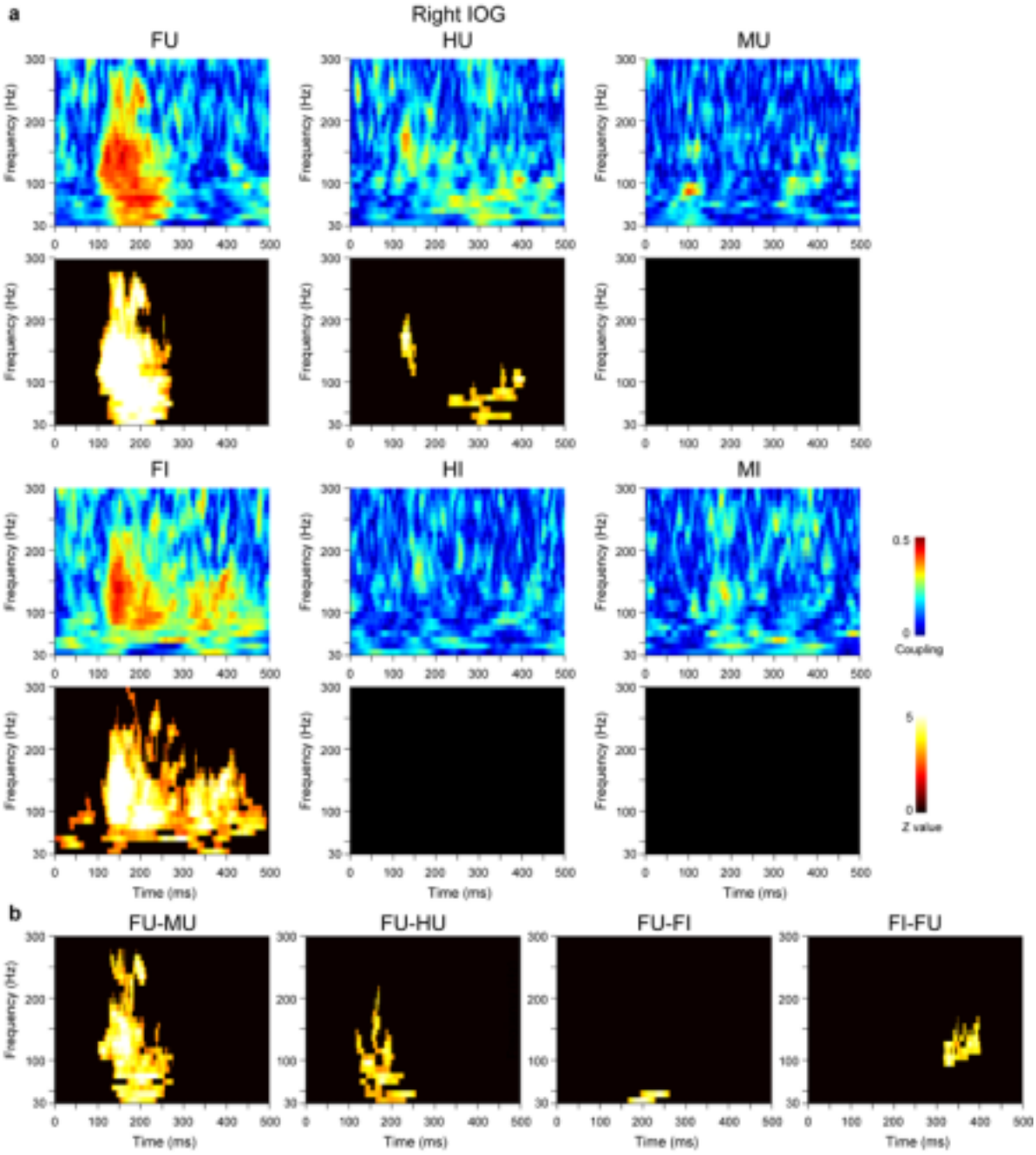

Fig. 5. (a) Theta–gamma cross-frequency coupling maps of right IOG activity and their statistical maps. FU = upright face; MU = upright mosaic; HU = upright house; FI = inverted face; MI = inverted mosaic; HI = inverted house. (b) Statistical maps for contrasts of right IOG theta–gamma cross-frequency couplings.

Table 5. Theta–gamma cross-frequency coupling regions showing significant right IOG activity.

	Activation Profile					
	Peak			Extent		
Contrast	Time (ms)	Frequency (Hz)	Z-Value	Time (ms)	Frequency (Hz)	Cluster Size (ms x Hz)
FU	156	130	7.60	96–276	30–270	3006
MU			n.s.			
HU	130	160	5.46	116–153	110–200	192
	394	100	5.06	228–408	30–120	551
FI	154	130	6.96	108–494	30–300	4886
	44	40	3.98	0–68	40–50	109
	73	80	3.77	33–94	70–120	135
MI			n.s.			
MU			n.s.			
FU - MU	164	140	5.99	101–276	30–270	2057
FU - HU	147	90	5.08	115–256	30–210	786
FU - FI	200	30	4.76	165–262	30–40	134
FI - FU	329	90	4.91	315–402	90–160	362
FI - MI	146	110	5.96	117–287	60–210	1105
	392	140	5.57	368–408	100–190	151
	329	100	5.19	228–408	90–170	201
FI - HI	138	130	6.24	121–175	50–220	449
	222	80	4.56	193–289	60–140	272
	386	130	4.44	366–414	110–170	133
	420	90	4.43	347–433	60–100	175
	346	140	4.21	297–355	90–150	209

FU = upright face; MU = upright mosaic; HU = upright house;

FI = inverted face; MI = inverted mosaic; HI = inverted house.

In the left IOG, there was no significant activation in any contrasts.

First, to describe the phenomenon, theta–gamma coupling patterns of IOG activity for each condition in each hemisphere were assessed using permutation tests. In the right IOG, rapid (96–276 ms) and broadband (30–270 Hz) gamma-band activity in response to upright faces was significantly associated with theta-band activity. No significant cross-frequency coupling was observed in response to upright mosaics, and two small clusters were found to be significant during 116–408 ms in response to upright houses in the right IOG. In response to inverted faces, as was true for upright faces, there was a rapid theta-associated gamma-band activation in the right IOG starting at 108 ms; however, as compared with upright faces, this activity was more prolonged and lasted until 494 ms. Some

additional small clusters of activation were also found at other time points. In response to inverted mosaics and inverted houses, there was no significant activation in the right IOG. In the left IOG, there was no significant theta–gamma coupling under any condition.

Then, face-specific cross-frequency coupling patterns of the IOG in each hemisphere were investigated using the contrasts of upright faces versus upright mosaics and upright faces versus upright houses. These contrasts consistently revealed significant clusters of rapid and broadband theta-associated gamma-band activity in the right IOG spanning 115–256 ms and 30–210 Hz. No significant cross-frequency coupling was found in the left IOG.

Next, effects of the inverted presentation of faces were tested using the contrast of upright versus inverted faces and inverted versus upright faces. The contrast of upright versus inverted faces led to significant theta–gamma coupling in the right IOG at 165–262 ms. The contrast of inverted versus upright faces induced a significant cluster of activity in the right IOG at a later time point during 315–402 ms. No significant cross-frequency coupling was found in the left IOG.

The contrasts of inverted faces versus inverted mosaics and inverted faces versus inverted houses were also tested. In the right IOG, as in the case of upright faces, these contrasts consistently revealed significant rapid (121–408 ms), broadband (60–210 Hz) theta–gamma coupling. In the left IOG, there was no significant cross-frequency coupling.

4. Discussion

The current ERP results identified the occurrence of a clear negative deflection in the IOG, specifically the right IOG, peaking at about 170 ms in response to upright faces relative to upright mosaics and houses. Additionally, compared with the upright presentation of faces, the inverted presentation of faces elicited a more evident and later negative deflection in this ERP component. These results are consistent with some previous intracranial EEG studies reporting that the negative deflection in the IOG in this time range was heightened in response to faces relative to other stimuli (e.g., Jonas et al., 2012) and enhanced and delayed in response to inverted faces as compared with upright faces (Rosburg et al., 2010). These data suggest that the stimuli used in this study activated the IOG in a comparable way to previous studies.

More importantly, the present results of the time–frequency analyses demonstrate that the IOG, specifically the right IOG, displayed stronger gamma-band activity in response to upright faces than to upright mosaics and houses as early as 110 ms. Because gamma oscillations reflect computational activity in local neural circuits (Buzsáki and Wang, 2012), the current findings suggest that the IOG conducts face processing at this early time stage. The rapid IOG gamma-band activation is in line with findings from a previous intracranial EEG study that analyzed the time–frequency profiles of IOG activity using non-facial stimuli (Tallon-Baudry et al., 2005). However, no study has fully investigated the time–frequency profile of IOG activity in response to faces. Although some previous scalp-recorded EEG/MEG studies conducted time–frequency analyses for neural activity during face processing, these studies did not detect gamma-band activity at 100 ms in the posterior cortices (e.g., Gao et al., 2013). It seems reasonable that the direct intracranial recording of field potentials in the IOG conducted in this study enhanced sensitivity to high-frequency neuronal activity (cf. Mukamel and Fried, 2012). It has been suggested that initial face processing in the cortex occurs at approximately 170 ms because several previous EEG/MEG studies found a negative deflection at this time point, which is considered to be the earliest robust face-specific component recorded on the scalp (e.g., Bentin et al., 1996; for a review, see Rossion and Jacques, 2008). To our knowledge, this is the first direct evidence that gamma-band activity in the IOG initiates face processing as early as 110 ms following after stimulus onset.

Our results showed that the gamma-band activities in the IOG at 100–200 ms were higher both for upright and inverted faces as compared with control stimuli and the activities for upright and inverted faces were not different evidently. Because previous behavioral studies showed that the inverted presentation of faces impairs the configural, but not featural, processing of faces (e.g., Farah et al., 1995), the IOG activity at this time stage appears to reflect the processing of facial features. Consistent with this notion, several previous stimulation (e.g., Pitcher et al., 2007) and neuroimaging (e.g., Liu et al., 2010) studies have identified the involvement of the IOG in the featural processing of faces. Some researchers have also theoretically proposed that the IOG is involved in early-stage featural processing of faces (e.g., Haxby et al., 2000). These data suggest that the IOG conducts the featural processing of faces at 100–200 ms, which is reflected by gamma oscillations.

The IOG also displayed heightened gamma-band activity in response to upright faces relative to upright mosaics and houses after 200 ms. As discussed below, the frequency profiles and cross-frequency coupling patterns differed between gamma-band activity at 100–200 ms and that at 200–500 ms. These results suggest that the IOG manages multiple processing stages for faces during a few hundred milliseconds.

Consistent with this notion, in contrast to activity during 100–200 ms, gamma-band activity in the IOG during 200–500 ms was heightened in response to upright faces relative to inverted faces. Based on behavioral evidence regarding the impaired configural visual processing of inverted faces (e.g., Farah et al., 1995), this activity appears to be the neural correlate of configural face processing. Several lesion (e.g., Rossion et al., 2003), stimulation (e.g., Jonas et al., 2012), and neuroimaging (e.g., Strother et al., 2011) studies have shown that the IOG was involved in the configural perception and identity recognition of faces. Based on these data, some researchers have proposed that the IOG is involved in late-stage configural processing of faces (e.g., Rossion et al., 2011). The present findings complement previous empirical and theoretical studies with temporal and frequency profiles indicating that gamma-band activity in the IOG during 200–500 ms is involved in the visual processing of facial configuration.

In addition to traditional gamma subband activity between 30 and 100 Hz (cf. Herrmann et al., 2010), the IOG exhibited higher gamma subband activity at 100–300 Hz in response to upright faces. Interestingly, the frequency profiles changed depending on time. Specifically, whereas early activation occurred at approximately 100–200 ms and included a broad range of 40–300 Hz, later activation primarily occurred within the frequency range of 100–200 Hz. Additionally, the effect of the presentation of inverted faces differed across gamma subbands. Specifically, lower activity was observed in response to inverted versus upright faces mainly in the higher as compared to the traditional gamma subband, which is consistent with previous studies indicating that different gamma subbands are related to different information-processing functions (e.g., Edwards et al., 2005; for a review, see Crone et al., 2006). Furthermore, several animal studies have reported that different gamma subbands reflect the activity of different neuronal ensembles (e.g., Chrobak et al., 2000; for a review, see Buzsáki and Wang, 2012). Collectively, these data suggest that face processing in the IOG

is implemented by multiple types of neuronal assemblies, each of which supports different computations and exhibits different time–frequency profiles.

Furthermore, the present results of cross-frequency coupling analyses revealed that the gamma-band activity amplitude was coupled with the phase of theta-band activity in response to upright faces during the 100–300 ms time period. This coupling was more evident in response to upright faces than to upright mosaics and houses. Several previous studies have shown that phase–amplitude cross-frequency coupling between theta- and gamma-band activities reflected neural network interactions between long-range inter-regional communication and local intra-regional computations (e.g., Liebe et al., 2012; for reviews, von Stein and Sarnthein, 2000; Canolty and Knight, 2010). Accordingly, it has been proposed that theta oscillations transmitted from other regions entrain local gamma oscillations (Canolty and Knight, 2010). Together with these previous data, the current results suggest that IOG gamma oscillations reflect face processing triggered by theta oscillation inputs from other brain regions. Because the onset of this cross-frequency coupling is very rapid, it is speculated that theta oscillations are first transmitted from early visual areas in a feedforward manner.

The cross-frequency coupling analyses conducted in this study revealed different patterns of activity in response to upright and inverted faces. The contrasts identified stronger theta–gamma coupling for upright faces relative to inverted faces at approximately 150–250 ms. Based on the aforementioned interpretation that the inverted presentation of faces impairs their configural processing, it is speculated that configural face processing is more efficiently triggered in response to upright faces, with feedforward inputs from early visual areas at this early time stage. In contrast, theta–gamma coupling of inverted faces occurred over a broader time range, approximately 100–500 ms, and it was stronger at approximately 300–400 ms. Regarding the processing of inverted faces, several previous neuroimaging studies have found a more widespread activation of brain regions in response to inverted faces compared to upright faces (e.g., Haxby et al., 1999; Joseph et al., 2006). Given the findings discussed above, it is speculated here that inverted faces may require prolonged computation and additional inter-regional communication at later stages to complement their lack of configural information.

The present data demonstrated that activity related to face processing was more evident in the

right than in the left IOG. This finding is consistent with several lines of neuropsychological (e.g., De Renzi et al., 1994), stimulation (e.g., Pitcher et al., 2007), neuroimaging (e.g., Kanwisher et al., 1997), and electrophysiological (e.g., Bentin et al., 1996) evidence and suggests that face processing in the IOG, as reflected by gamma oscillations, is dominant in the right hemisphere. However, it must be noted that electrode placement in the present study was based solely on anatomical information. Therefore, it is possible that the electrodes in the right and left IOG were not comparable in regard to their physiological activity and associated information-processing functions. Further investigation is necessary to determine whether hemispheric functional asymmetry exists with respect to face processing in the IOG.

The current findings have implications for some issues related to neural processing of faces. First, our results revealing the rapid activation of the IOG suggest that the cortical visual areas may have the potential to rapidly process facial stimuli. This issue is particularly important for the processing of emotional facial expressions. Behavioral studies have shown that, among the information in faces, emotional significance could be processed the most rapidly (e.g., Murphy et al., 1993). Neuroimaging studies have suggested that such rapid emotional expression processing is related to amygdala activity (e.g., Morris et al., 1998). Indeed, an intracranial EEG study has revealed that amygdala activation for emotional facial expressions occurred at approximately 100 ms from stimulus onset (Sato et al., 2011). Some researchers speculated that the rapid amygdala activation in response to emotional expressions might be accomplished via the subcortical visual pathways involving the pulvinar and superior colliculus bypassing the cortical visual areas (e.g., Tamietto and de Gelder, 2010), whereas other researchers proposed that the cortical visual areas might process facial information prior to amygdala activation and send input to the amygdala (Pessoa and Adolphs, 2010). Our findings indicate that the IOG activation in response to faces occurred as early as the time of amygdala activation in response to emotional facial expressions (Sato et al., 2011) and suggest that the IOG might be able to provide facial information to the amygdala. Testing the timing and correlation of the activation of these brain regions would provide crucial evidence for revealing the information flow between the visual cortex and the amygdala in the early stages of facial expression processing.

Second, our data showing IOG involvement both in featural and configural processes for faces

suggest that a single brain region might be involved in multiple computations to process facial information. The results are consistent with previous lesion studies showing that both featural and configural processing of faces were impaired in some brain-damaged patients (e.g., Barton et al., 2002; Barton and Cherkasova, 2003). The results are also consistent with some computer simulation studies for face recognition showing that a single computational mechanism implemented both local and global processing of facial images (e.g., Križaj et al., 2010; Liao et al., 2013), and the theoretical suggestion that the brain conducts inter-regional iterative matching processes to accomplish visual recognition (Friston, 2005). In contrast with traditional feedfoward face-processing models (e.g., Bruce and Young, 1986; Haxby et al., 2000), recent lesion studies suggest that feedback activation of the IOG plays a crucial role in the processing of faces (Rossion, 2008). Further investigation of the relationships between information processing and neural spatiotemporal activation is an important matter for future research.

Finally, our data showing the involvement of IOG in face processing suggest the critical influence of IOG malfunctioning. Previous studies have shown that impaired face processing is a core symptom of some psychiatric disorders such as autism spectrum disorders (e.g., Langdell, 1978) and schizophrenia (e.g., Shin et al., 2008). Some recent electrophysiological studies have suggested that the neural underpinnings of these disorders include impairments in local gamma oscillations and long-range communication via theta–gamma coupling (e.g., Kirihara et al., 2012). Together with these data, we speculate that problems in the gamma oscillations and their theta couplings in the IOG might underlie the face-processing deficits in these psychiatric disorders, which may be demonstrated by intracranial EEG recordings in patients (e.g., Rutishauser et al., 2013).

One limitation of this study is that all participants were patients with epilepsy. Although the visual inspection of MRI data confirmed the absence of anatomical abnormalities in the IOG of these patients, their long-lasting pathological states may have affected their face processing abilities. However, a previous study investigating face recognition in epileptic patients reported that patients were impaired in the long-term memory for faces but not in the immediate recognition of faces (Hötting et al., 2010). These data seem to suggest that epileptic activity has little influence on the immediate processing of faces, particularly with reference to cortical visual areas. Further studies

involving noninvasive electrophysiological recordings in normal participants should confirm this idea and strengthen the current findings.

In summary, findings from the current intracranial field potential recordings in humans provide a new understanding of the electric neuronal activity in the IOG during face processing. The results from time–frequency analyses revealed greater gamma-band activity in the right IOG, starting at approximately 110 ms and covering 40–300 Hz, in response to upright faces as compared with upright mosaics and houses. Phase–amplitude cross-frequency coupling analyses showed that the gamma-band activity was more evidently coupled with theta-band activity at 100–250 ms when processing faces compared with houses and mosaics. Relative to upright faces, gamma-band activity related to inverted faces was comparable at 100–200 ms but was weaker and differentially coupled with theta–band activity after 200 ms. These results suggest that, in collaboration with theta oscillations transmitted from other brain regions, broadband gamma oscillations in the right IOG conduct rapid and multistage (i.e., both featural and configural) face processing.

Conflicts of interest

The authors declare that they have no conflict of interest.

Funding

This study was supported by funds from the Benesse Corporation, the Organization for Promoting Research in Developmental Disorders, and JSPS Funding Program for Next Generation World-Leading Researchers (No. LZ008).

References

Adrian ED. Olfactory reactions in the brain of the hedgehog. Journal of Physiology, 100(4):459–473, 1942.

Allison T, Ginter H, McCarthy G, Nobre AC, Puce A, Luby M, and Spencer DD. Face recognition in human extrastriate cortex. Journal of Neurophysiology, 71(2):821–825, 1994.

Allison T, Puce A, Spencer DD, and McCarthy G. Electrophysiological studies of human face

perception. I: Potentials generated in occipitotemporal cortex by face and non-face stimuli. Cerebral Cortex, 9(5):415–430, 1999.

Ashburner J and Friston KJ. Unified segmentation. Neuroimage, 26(3):839–51, 2005.

Bartlett JC, Searcy J, and Abdi H. What are the routes to face recognition? In Peterson MA, Rhodes G. (Eds), Perception of faces, objects, and scenes: Analytic and holistic processing, Oxford: Oxford University Press, 2003: 21–52.

Bentin S, Allison T, Puce A, Perez E, and McCarthy G. Electrophysiological studies of face perception in humans. Journal of Cognitive Neuroscience, 8(6):551–565, 1996.

Berens P. CircStat: A Matlab toolbox for circular statistics. Journal of Statistical Software, 31(10):1–21, 2009.

Bouvier SE and Engel SA. Behavioral deficits and cortical damage loci in cerebral achromatopsia. Cerebral Cortex, 16(2):183–191, 2006.

Barton JJ and Cherkasova M. Face imagery and its relation to perception and covert recognition in prosopagnosia. Neurology, 61(2):220–225, 2003.

Barton JJ, Press DZ, Keenan JP, and O'Connor M. Lesions of the fusiform face area impair perception of facial configuration in prosopagnosia. Neurology, 58(1):220–225, 2002.

Bruce V, Young AW. Understanding face recognition. British Journal of Psychology, 77(3):305–327, 1986.

Buzsáki G and Wang XJ. Mechanisms of gamma oscillations. Annual Review of Neuroscience, 35:203–225, 2012.

Canolty RT, Edwards E, Dalal SS, Soltani M, Nagarajan SS, Kirsch HE, Berger MS, Barbaro NM, and Knight RT. High gamma power is phase-locked to theta oscillations in human neocortex. Science, 313(5793):1626–1628, 2006.

Canolty RT and Knight RT. The functional role of cross-frequency coupling. Trends in Cognitive Sciences, 14(11):506–515, 2010.

Chrobak JJ, Lorincz A, and Buzsáki G. Physiological patterns in the hippocampo-entorhinal cortex system. Hippocampus, 10(4):457–465, 2000.

Crone NE, Sinai A, and Korzeniewska A. High-frequency gamma oscillations and human brain

mapping with electrocorticography. Progress in Brain Research, 159:275–295, 2006.

De Renzi E, Perani D, Carlesimo GA, Silveri MC, and Fazio F. Prosopagnosia can be associated with damage confined to the right hemisphere: An MRI and PET study and a review of the literature. Neuropsychologia, 32(8):893–902, 1994.

Delorme A and Makeig S. EEGLAB: An open source toolbox for analysis of single-trial EEG dynamics including independent component analysis. Journal of Neuroscience Methods, 134(1):9–21, 2004.

Davies-Thompson J and Andrews TJ. Intra- and interhemispheric connectivity between face-selective regions in the human brain. Journal of Neurophysiology, 108(11):3087-3095, 2012.

Edwards E, Soltani M, Deouell LY, Berger MS, and Knight RT. High gamma activity in response to deviant auditory stimuli recorded directly from human cortex. Journal of Neurophysiology, 94(6):4269–4280, 2005.

Edwards E, Soltani M, Kim W, Dalal SS, Nagarajan SS, Berger MS, and Knight RT. Comparison of time–frequency responses and the event-related potential to auditory speech stimuli in human cortex. Journal of Neurophysiology, 102(1):377–386, 2009.

Engell AD and McCarthy G. Selective attention modulates face-specific induced gamma oscillations recorded from ventral occipitotemporal cortex. Journal of Neuroscience, 30(26):8780-8786, 2010.

Farah MJ, Tanaka JW, and Drain HM. What causes the face inversion effect? Journal of Experimental Psychology: Human Perception and Performance, 21(3):628–634, 1995.

Foucher JR, Otzenberger H, and Gounot D. The BOLD response and the gamma oscillations respond differently than evoked potentials: an interleaved EEG–fMRI study. BMC neuroscience, 4(22):2003.

Friston K. A theory of cortical responses. Philosophical Transactions of the Royal Society of London. Series B, Biological Sciences. 360(1456):815–836, 2005.

Friston KJ, Penny W, Phillips C, Kiebel S, Hinton G, and Ashburner J. Classical and Bayesian inference in neuroimaging: Theory. Neuroimage, 16(2):465–483, 2002.

Gao Z, Goldstein A, Harpaz Y, Hansel M, Zion-Golumbic E, and Bentin S. A

magnetoencephalographic study of face processing: M170, gamma-band oscillations and source localization. Human Brain Mapping, 34(8):1783–1795, 2013.

Haxby JV, Hoffman EA, and Gobbini MI. The distributed human neural system for face perception. Trends in Cognitive Sciences, 4(6): 223–233, 2000.

Haxby JV, Ungerleider LG, Clark VP, Schouten JL, Hoffman EA, and Martin A. The effect of face inversion on activity in human neural systems for face and object perception. Neuron, 22(1):189–199, 1999.

Herrmann CS, Fründ I, and Lenz D. Human gamma-band activity: A review on cognitive and behavioral correlates and network models. Neuroscience and Biobehavioral Reviews, 34(7):981–992, 2010.

Hötting K, Katz-Biletzky T, Malina T, Lindenau M, and Bengner T. Long-term versus short-term memory deficits for faces in temporal lobe and generalized epilepsy patients. Journal of the International Neuropsychological Society, 16(3):574–578, 2010.

Jonas J, Descoins M, Koessler L, Colnat-Coulbois S, Sauvée M, Guye M, Vignal JP, Vespignani H, Rossion B, and Maillard L. Focal electrical intracerebral stimulation of a face-sensitive area causes transient prosopagnosia. Neuroscience, 222:281–288, 2012.

Joseph JE, Gathers AD, Liu X, Corbly CR, Whitaker SK, and Bhatt RS. Neural developmental changes in processing inverted faces. Cognitive, Affective, & Behavioral Neuroscience, 6(3):223–235, 2006.

Kanwisher N, McDermott J, and Chun MM. The fusiform face area: a module in human extrastriate cortex specialized for face perception. Journal of Neuroscience, 17 (11):4302–4311, 1997.

Kilner JM and Friston KJ. Topological inference for EEG and MEG. Annals of Applied Statistics, 4(3):1272–1290, 2010.

Kilner JM, Kiebel SJ, and Friston KJ. Applications of random field theory to electrophysiology. Neuroscience Letters, 374(3):174–178, 2005.

Kingstone A, Friesen CK, and Gazzaniga MS. Reflexive joint attention depends on lateralized cortical connections. Psychological Science, 11(2):159–166, 2000.

Kirihara K, Rissling AJ, Swerdlow NR, Braff DL, and Light GA. Hierarchical organization of gamma

and theta oscillatory dynamics in schizophrenia. Biological Psychiatry, 71(10):873–880, 2012.

Klopp J, Halgren E, Marinkovic K, and Nenov V. Face-selective spectral changes in the human fusiform gyrus. Clinical Neurophysiology, 110(4):676–682, 1999.

Križaj J, Štruc V, Pavešić N. Adaptation of SIFT features for robust face recognition. Lecture Notes in Computer Science. 6111: 394–40, 2010.

Lachaux JP, George N, Tallon-Baudry C, Martinerie J, Hugueville L, Minotti L, Kahane P, and Renault B. The many faces of the gamma band response to complex visual stimuli. Neuroimage, 25(2):491–501, 2005.

Lachaux JP, Rodriguez E, Martinerie J, and Varela FJ. Measuring phase synchrony in brain signals. Human Brain Mapping, 8(4):194-208, 1999.

Lachaux JP, Rudrauf D, and Kahane P. Intracranial EEG and human brain mapping. Journal of Physiology, Paris, 97(4–6):613–628, 2003.

Langdell T. Recognition of faces: An approach to the study of autism. Journal of Child Psychology and Psychiatry and Allied Disciplines, 19(3):255–268, 1978.

Liao S, Jain AK, and Li SZ. Partial face recognition: Alignment-free approach. IEEE Transactions on Pattern Analysis and Machine Intelligence, 35(5):1193–1205, 2013.

Liebe S, Hoerzer GM, Logothetis NK, and Rainer G. Theta coupling between V4 and prefrontal cortex predicts visual short-term memory performance. Nature Neuroscience, 15(3):456–462, 2012.

Lisman JE and Jensen O. The theta–gamma neural code. Neuron, 77(6):1002–1016, 2013.

Litvak V, Mattout J, Kiebel S, Phillips C, Henson R, Kilner J, Barnes G, Oostenveld R, Daunizeau J, Flandin G, Penny W, and Friston K. EEG and MEG data analysis in SPM8. Computational Intelligence and Neuroscience, 852961. 2011.

Liu J, Harris A, and Kanwisher N. Perception of face parts and face configurations: An FMRI study. Journal of Cognitive Neuroscience, 22(1):203–211, 2010.

Makeig S, Debener S, Onton J, and Delorme A. Mining event-related brain dynamics. Trends in Cognitive Sciences, 8(5):204–210, 2004.

McKelvie, S J. Emotional expression in upside-down faces: Evidence for configurational and componential processing. British Journal of Social Psychology, 34(3):325–334, 1995.

Mihara T and Baba K. Combined use of subdural and depth electrodes. In Luders HO, Comair YG. (Eds), Epilepsy Surgery (second ed.), Philadelphia, PA: Lippincott Williams and Wilkins, 2001: 613–621.

Mondloch CJ, Le Grand R, and Maurer D. Configural face processing develops more slowly than featural face processing. Perception, 31(5):553–566, 2002.

Morris JS, Öhman A, and Dolan RJ. Conscious and unconscious emotional learning in the human amygdala. Nature, 393(6684):467–470, 1998.

Mukamel R and Fried I. Human intracranial recordings and cognitive neuroscience. Annual Review of Psychology, 63:511–537, 2012.

Murphy ST and Zajonc RB. Affect, cognition, and awareness: Affective priming with optimal and suboptimal stimulus exposures. Journal of Personality and Social Psychology, 64(5):723–739, 1993.

Oldfield RC. The assessment and analysis of handedness: the Edinburgh inventory. Neuropsychologia, 9(1):97–113, 1971.

Oswal A, Litvak V, Sauleau P, and Brown P. Beta reactivity, prospective facilitation of executive processing, and its dependence on dopaminergic therapy in Parkinson's disease. Journal of Neuroscience, 32(29):9909–9016, 2012.

Pessoa L and Adolphs R. Emotion processing and the amygdala: From a 'low road' to 'many roads' of evaluating biological significance. Nature Review Neuroscience, 11(11):773–783, 2010.

Pitcher D, Walsh V, and Duchaine B. The role of the occipital face area in the cortical face perception network. Experimental Brain Research, 209(4):481–493, 2011.

Pitcher D, Walsh V, Yovel G, and Duchaine B. TMS evidence for the involvement of the right occipital face area in early face processing. Current Biology, 17(18):1568–1573, 2007.

Purcell DG and Stewart AL. The face-detection effect. Bulletin of the Psychonomic Society, 24(2):118–120, 1986.

Rosburg T, Ludowig E, Dümpelmann M, Alba-Ferrara L, Urbach H, and Elger CE. The effect of face

inversion on intracranial and scalp recordings of event-related potentials. Psychophysiology, 47(1):147–157, 2010.

Rossion B. Constraining the cortical face network by neuroimaging studies of acquired prosopagnosia. Neuroimage, 40:423–426, 2008.

Rossion B, Caldara R, Seghier M, Schuller AM, Lazeyras F, and Mayer E. A network of occipito-temporal face-sensitive areas besides the right middle fusiform gyrus is necessary for normal face processing. Brain, 126(11):2381–2395, 2003.

Rossion B, Dricot L, Goebel R, and Busigny T. Holistic face categorization in higher order visual areas of the normal and prosopagnosic brain: Toward a non-hierarchical view of face perception. Frontiers in Human Neuroscience, 4:225. 2011.

Rossion B and Jacques C. Does physical interstimulus variance account for early electrophysiological face sensitive responses in the human brain? Ten lessons on the N170. Neuroimage, 39(4):1959–1979, 2008.

Rutishauser U, Tudusciuc O, Wang S, Mamelak AN, Ross IB, and Adolphs R. Single-neuron correlates of atypical face processing in autism. Neuron, 80(4):887–899, 2013.

Sato W, Kochiyama T, Uono S, Matsuda K, Usui K, Inoue Y, and Toichi M. Rapid amygdala gamma oscillations in response to fearful facial expressions. Neuropsychologia, 49(4): 612–617, 2011.

Sato W, Kochiyama T, Uono S, Matsuda K, Usui K, Inoue Y, and Toichi M. Temporal profile of amygdala gamma oscillations in response to faces. Journal of Cognitive Neuroscience, 24(6):1420–1433, 2012.

Scheffer-Teixeira R, Belchior H, Caixeta FV, Souza BC, Ribeiro S, and Tort AB. Theta phase modulates multiple layer-specific oscillations in the CA1 region. Cerebral Cortex, 22(10):2404–2414, 2012.

Sergent J, Ohta S, and MacDonald B. Functional neuroanatomy of face and object processing. A positron emission tomography study. Brain, 115(1):15–36, 1992.

Shin YW, Na MH, Ha TH, Kang DH, Yoo SY, and Kwon JS. Dysfunction in configural face processing in patients with schizophrenia. Schizophrenia Bulletin, 34(3):538–543, 2008.

Strother L, Mathuranath PS, Aldcroft A, Lavell C, Goodale MA, and Vilis T. Face inversion reduces the persistence of global form and its neural correlates. PLoS One, 6(4):e18705. 2011.

Tallon-Baudry C, Bertrand O, Delpuech C, and Pernier J. Stimulus specificity of phase-locked and non-phase-locked 40 Hz visual responses in human. Journal of Neuroscience, 16(13):4240–4249, 1996.

Tallon-Baudry C, Bertrand O, Hénaff MA, Isnard J, and Fischer C. Attention modulates gamma-band oscillations differently in the human lateral occipital cortex and fusiform gyrus. Cerebral Cortex, 15(5):654–662, 2005.

Tamietto M and de Gelder B. Neural bases of the non-conscious perception of emotional signals. Nature Review Neuroscience, 11(10):697–709, 2010.

Tort AB, Scheffer-Teixeira R, Souza BC, Draguhn A, and Brankačk J. Theta-associated high-frequency oscillations (110–160Hz) in the hippocampus and neocortex. Progress in Neurobiology, 100:1–14, 2013.

Tottenham N, Leon AC, and Casey BJ. The face behind the mask: A developmental study. Developmental Science, 9(3):288–294, 2006.

von Stein A, and Sarnthein J. Different frequencies for different scales of cortical integration: From local gamma to long range alpha/theta synchronization. International Journal of Psychophysiology, 38(3):301–313, 2000.

Voytek B, D'Esposito M, Crone N, and Knight RT. A method for event-related phase/amplitude coupling. Neuroimage, 64:416–424, 2013.

Worsley KJ, Marrett S, Neelin P, Vandal AC, Friston KJ, and Evans AC. A unified statistical approach for determining significant signals in images of cerebral activation. Human Brain Mapping, 4(1):58–73, 1996.

Yin RK. Looking at upside-down faces. Journal of Experimental Psychology, 81(1):141–145, 1969.

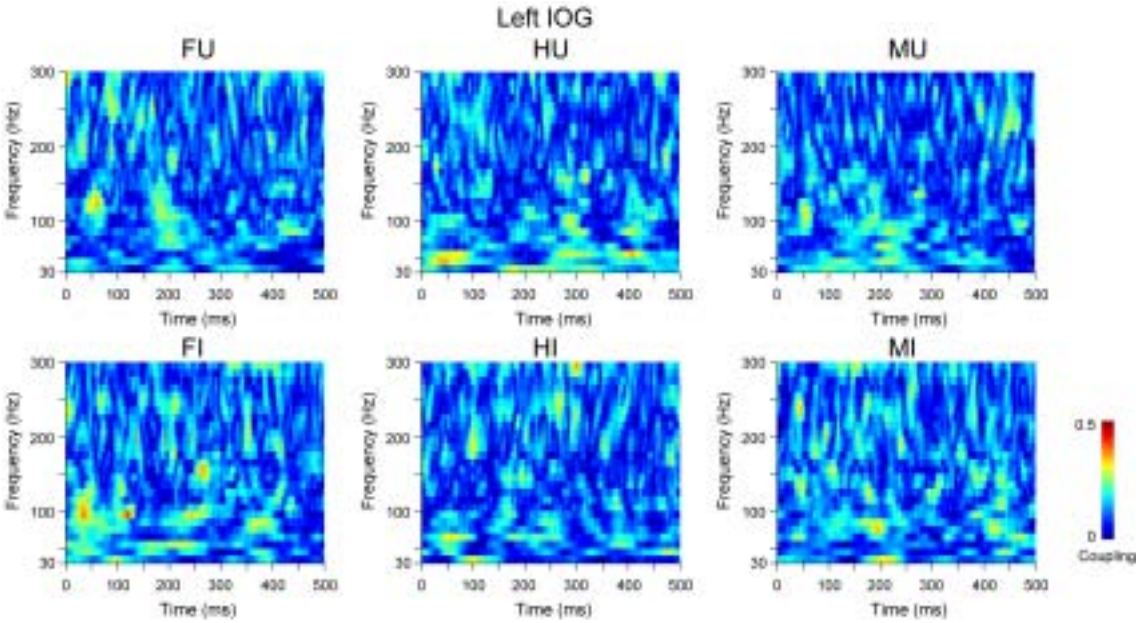

Supplementary Fig. 1. Theta–gamma cross-frequency coupling maps of left IOG activity. FU = upright face; MU = upright mosaic; HU = upright house; FI = inverted face; MI = inverted mosaic; HI = inverted house.